

CONTRACT N°: RII3-CT-2004-506065

ISSUE CERTIFICATE

EURONS

EUROpean Nuclear Structure research

Activity JRA11 - TRAPSPEC

Identification: D-J11-1.1

Revision: 0

Report on task T-J11-1
(Simulations and calculations)

Dissemination level: *PU*Issued by: *U-Mainz / KU-Leuven*Reference: *EURONS-D-J11-1.1*Status: *Final***Summary:**

We performed different calculations and simulations that are necessary for optimal experimental development and data analysis in the aSPECT experiment. The calculations included i) electromagnetic computations for optimized electrode and coil design, design of magnetic shielding, etc., ii) trajectory calculations of charged particles in electromagnetic fields, iii) scattering calculations of charged particles with gas molecules/atoms and with solid materials, iv) calculations for understanding the background processes of trapped particles, and v) calculations for better understanding various systematic effects.

| | | | |
|------------|--|--|--|
| 31.12.2008 | Werner Heil U-Mainz | Werner Heil U-Mainz | Nathal Severijns, KU-Leuven |
| | | | |
| DATE | RESPONSIBLE Name/Company Signature | WP LEADER Name/Company Signature | COORDINATOR Name/Company Signature |

**Report for the TRAPSPEC JRA-11 in EURONS
on task T-J11-1
(Simulations and calculations)**

Motivation

The purpose of the retardation spectrometer aSPECT is to determine the antineutrino electron angular correlation coefficient a with high precision, by measuring the integral proton spectrum in free neutron decay. With a precise measurement of the correlation coefficient a tests of the validity of the Standard Model become possible. Of great interest are here the searches for scalar and tensor interactions, and to test the unitarity of the CKM matrix.

3-dimensional electric field calculations {Subtask T-J11-1.1. Design-Optimization}

A C-program package for general 3-dimensional electric field calculation was written, and this was then applied for electric field calculation of the aSPECT electrode system. The boundary element (charge density) method was used. In this method, first one has to discretize the electrode system into small subelements, in our program package these are rectangles. The program can compute the electric potential of a general rectangular subelement with constant charge density at an arbitrary field point. The charge densities of the subelements can be computed by solving a linear algebraic equation system. Knowing the charge densities, one can compute the electric potential at a field point by summing the potential contributions from all subelements (Fig. 1).

The boundary element method has the following restrictions. In order to compute the N charge densities, one has to compute the $N \times N$ Coulomb matrix, with N^2 matrix elements, and all these elements have to fit into the main memory of the computer. Therefore, with 1 GB memory the maximal number of charge densities is about 10000. In addition, the computation time for the solution of the linear algebraic equation system increases with the third power of N , and this fact limits also the number of charge densities practically below 20000. Nevertheless, this constraint presents no problem for the aSPECT electrode system computation.

For the trajectory calculation, the field has to be computed at many points, therefore the field calculation has to be fast. We have used various field computation methods. First, the electric field can be computed from the potential by numerical differentiation. If we have many electrode subelements (f.e. a few thousand), the potential calculation by summation over all subelements is quite slow, and then the field calculation is even slower. Therefore, we had to find some methods to increase the field computation speed. One possibility was to approximate (for the purpose of the field calculation) each subelement rectangle by a charged point, and compute the electric field by summing the contributions from all these charged points. This method is much faster than the previously described

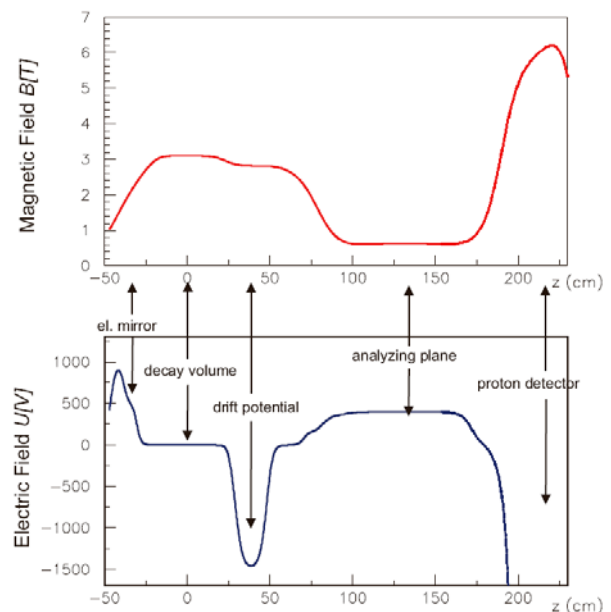


Figure 1: Electrostatic potential (blue line) and magnetic field (red line) along the z -axis of the aSPECT spectrometer.

one. Unfortunately, close to the electrode surfaces this method is not accurate enough. Nevertheless, the flux tube of the aSPECT electrode system (where we have to compute the proton trajectories) has a few cm distance from the electrodes. In addition, one could increase the accuracy by taking more points (in this case we need more computation time). Further details about the electric field calculations can be found in [2,4,6,13].

Magnetic field calculations {Subtask T-J11-1.1. Design-Optimization}

The proton trajectory calculations need also the magnetic field. In our approach, the magnetic field is mainly computed by zonal harmonic (Legendre polynomial) expansion. This method is much faster (by a few hundred times) than the generally used calculation method with elliptic integrals. The expansion is not convergent close to the coils, but the field points during the trajectory calculations are all far from the coils. Further details about the magnetic field calculations can be found in [2,5,13]. The design calculations (Figs. 1 and 2) and measurements (Fig. 2) are described in the diploma thesis of F. Ayala Guardia [12].

In addition to trajectory calculations, an optimization calculation was made, in order to find an optimal geometry for a pair of air coils around the aSPECT spectrometer. This air coil was necessary in order to compensate the magnetic field inhomogeneity due the superconducting coils at the analyzing plane (Fig. 3). The magnetic field shape after corrections fulfils the requirements (field shape is as expected with an uncertainty of $\Delta B/B \sim 10^{-4}$).

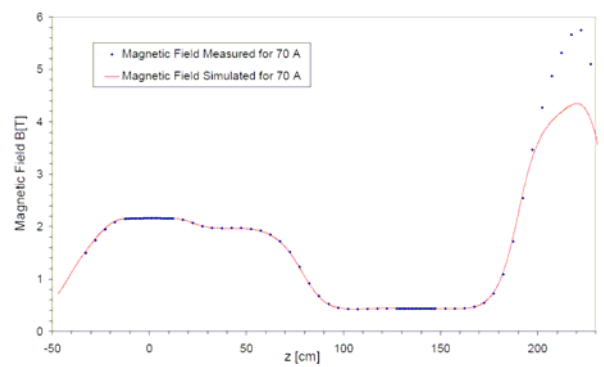


Figure 2: Theoretic simulation of the magnetic field profile in the z-axis (red line), and measured magnetic field profile (blue points). Both series correspond to a magnet current set to 70 A, which corresponds to 70% of maximum magnetic field. The Hall probe calibration ends at 2.2 T.

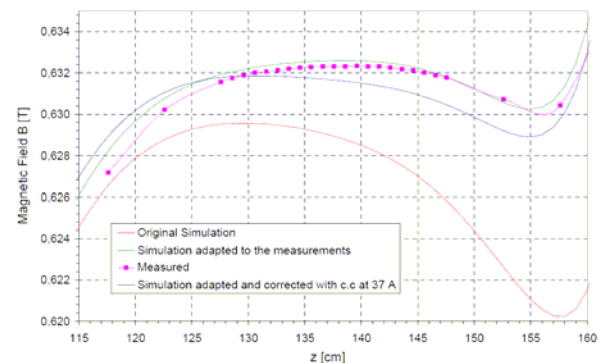


Figure 3: Magnetic field correction by means of the air coils. The red line is the original simulation and the pink points are the measured values. The green line is the simulated magnetic field corrected to fit with the measurements and the blue line is the corrected magnetic field. The main magnet is simulated to be charged with a current of 100 A.

In a recent beam time performed during April / May 2008 at the Institut Laue-Langevin, several systematic effects were investigated experimentally. Therefore, an additional optimization calculation was made, in order find an optimal geometry for a second pair of air coils around the aSPECT spectrometer (Fig. 4, picture on the left). This air coil was needed in order to change the ratio of the magnetic fields in the analysing plane (B_A) and the decay volume (B_0), $r_B = B_A / B_0$. Investigation of this systematic effect showed that the antineutrino electron angular correlation coefficient a_{exp} changes with the magnetic field ratio r_B as described by a slightly different response function $F_{tr}(E)$ (Fig. 4, graph on the right, and cf. report on task T-J11-8).

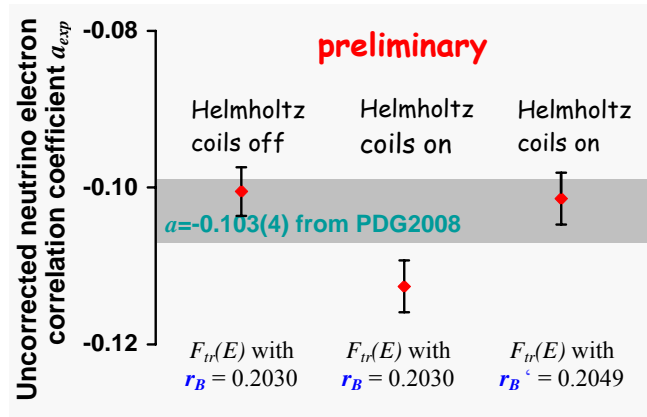
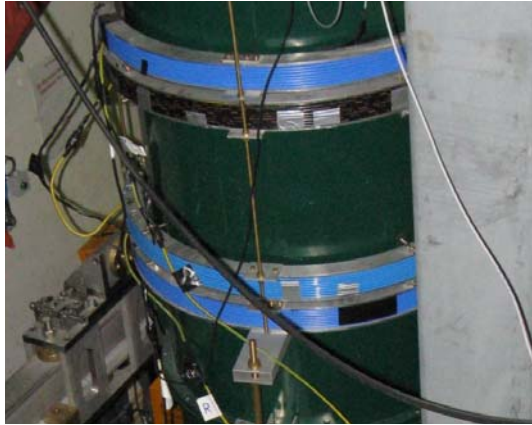


Figure 4: Left: Inner air coils around the aSPECT spectrometer to compensate the magnetic field inhomogeneity and outer air coils to change the magnetic field ratio r_B , respectively. Right: Determination of a_{exp} for two different settings (Helmholtz coils off, $r_B = 0.2030$, and Helmholtz coils on, $r_B = 0.2049$). The second point of the graph has been determined assuming Helmholtz coils of ($r_B = 0.2030$), and it results in a systematic shift in a_{exp} . For comparison, the present literature value is shown with its error band.

Magnetic shielding and effect of magnetic materials {Subtask T-J11-1.1. Design-Optimization}

COMSOL Multiphysics Electromagnetics Module¹ was successfully used to model and optimize an anti-magnetic screen for the aSPECT spectrometer to obtain a design that reduces the exterior magnetic field by a factor of about 10, that does not affect the internal magnetic field and its homogeneity, and that makes sure that the additional forces onto the superconducting coils are non-destructive.

A closed cylinder made of ordinary sheet iron (length 400 cm, diameter 190 cm, thickness 10 cm), what corresponds to a mass of 20 tons, would provide big enough shield factor² (Fig. 5), but the support of the spectrometer is very difficult, and for a box one expects a lower but still sufficient large shield factor. Thus, availability and price of ferromagnetic materials suggest using a box instead of the cylinder.

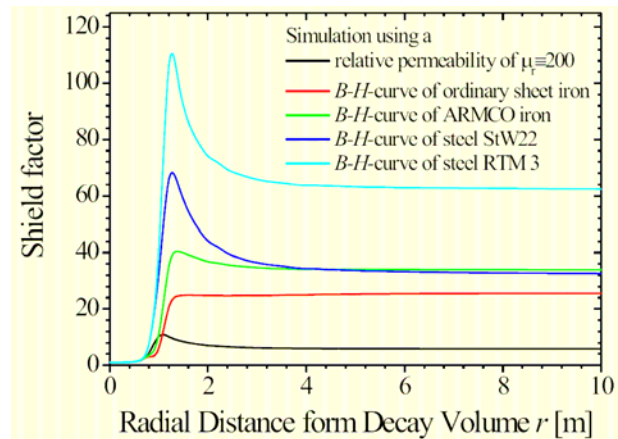


Figure 5: Shield factor for a closed cylinder of a mass of 20 tons for different magnetic materials.

On the basis of the electromagnetic force calculations (Fig. 6, simulation on the left) the aSPECT spectrometer was centred inside the anti-magnetic screen.

The setup of the aSPECT spectrometer inside the anti-magnetic screen is shown in Fig. 6 (picture on the right). The shield provides a sufficient reduction of the exterior magnetic field (Fig. 7). Further details about the design of the anti-magnetic screen can be found in [8,11].

¹ A package that extends the finite element method modelling environment and is functionality optimized for the 3-dimensional analysis of electromagnetic effects, components and systems, and can be found at <http://www.comsol.eu>.

² Shield factor defined as the ratio of the magnetic fields in radial direction without and with shield.

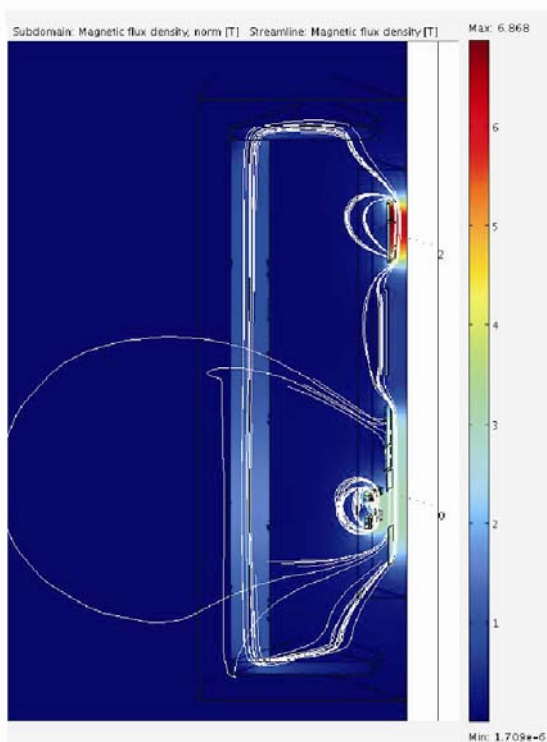


Figure 6: Left: The magnetic field in the symmetry plane that cuts through a pillar of the anti-magnetic screen. Right: Setup of aSPECT inside the shield, a combination of construction steel (plates of cross-section 180x180cm² and thickness 10cm) and ARMCO iron (pillars of cross-section 20x20cm² and length 400cm).

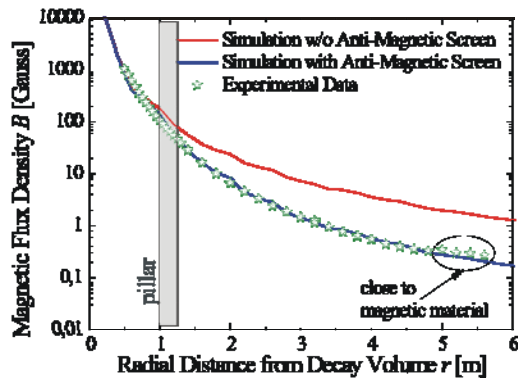


Figure 7: Influence on the exterior magnetic field: The magnetic field in radial direction, without (red) and with anti-magnetic screen (blue line). The green stars indicate a measurement between two pillars of the anti-magnetic screen

Trajectory calculations {Subtask T-J11-1.1. Design-Optimization / Subtask T-J11-1.2. Systematic effects }

For the proton trajectory calculations an 8th order Runge-Kutta program was used. This calculation method combines high numerical accuracy with high computational speed. Using this method, together with the very precise field calculation, one can easily obtain a relative accuracy for the energy conservation that is better than 10⁻¹⁰. The proton trajectory calculation was used for the evaluation of various systematic effects: adiabaticity, edge effect, magnetron drift in the electric dipole field, and calculations of rest gas effects. Further details about the trajectory calculations can be found in [13], and about the systematic effects in [9,10,13].

Penning traps, Penning discharge {Subtask T-J11-1.2. Systematic effects}

In some aSPECT experiments, relatively strong discharge phenomena have been observed. These discharges could be due field emission processes, near the detector, where high electric field is present. On the other hand, the aSPECT electrode system contains several Penning traps (both for electrons and for positive ions). These traps could cause also serious discharge processes. In order to understand these processes, the literature of the Penning discharge phenomenon was studied, and various calculations were performed, to search for various traps, which could be responsible for the discharge and background processes observed in the aSPECT experiment.

The Penning discharge is in some respect similar to the Townsend discharge, which occurs for relatively high pressure. On the other hand, although both the vacuum breakdown and the Penning discharge are present even at very good vacuum conditions, the physics of Penning discharge is completely different from vacuum breakdown. The main difference is that the Penning discharge occurs only in presence of magnetic field, and it requires stable charged particle trapping (mainly electrons). The trapped electrons can suffer ionizational collisions with the residual gas molecules (even with high vacuum of order 10^{-9} mbar), and the positive ions, hitting the anode, can produce more electrons by secondary emission.

A detailed comparison of the aSPECT discharge phenomena with discharges of other experiments (neutrino mass experiments of Mainz and KATRIN) has been performed, and Penning traps in the aSPECT electrode system have been searched. Three main trapping regions have been found: in the bottom part of the spectrometer (mirror electrodes), at the analyzing plane, and near the detector. At the mirror electrode a wire system was installed (Fig. 8), in order to prevent electron trapping. At the detector a different dipole electrode was installed (cf. report on task T-J11-8, Figs. 8 to 10), and the detector potential was decreased (cf. report on task T-J11-8, Figs. 11,12), to avoid the deep traps that were present in earlier versions of the experiment. The Penning traps at the analyzing plane could not be changed, because these traps are absolutely necessary for the electric retardation method of the proton spectrum measurement. In addition, the traps at the analyzing plane are only a few hundred V deep.

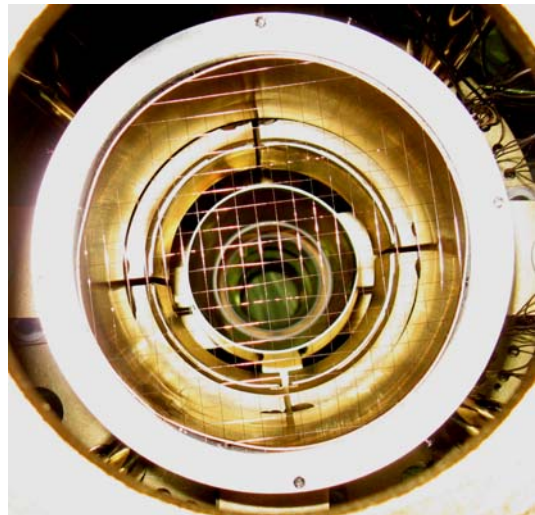


Figure 8: Wire system installed at the mirror electrode, during a recent beam time at the Institut Laue-Langevin during April / May 2008, in order to prevent electron trapping.

Further details about the Penning traps and discharges can be found in [7,10,13]. For investigations of penning discharges causing fake effects (voltage dependent background signal) in the proton spectrum cf. report on task T-J11-8 (Fig. 13) and [9,10].

Detector efficiency {Subtask T-J11-1.2. Systematic effects}

Detector imperfections, namely the backscattering of protons in the detector, lead to a distortion of the measured proton spectrum, as it causes the detection efficiency to depend on the proton impact energy and impact angle [13].

For our test beam time taken at the FRM-II reactor in Munich, we performed new simulations using the software package SRIM 2006³, because it was reported that its previously used version underestimates the scattering at low energies. The average energy loss in the dead

³ A program, which simulates the stopping and range of ions in matter and can be found at <http://www.srim.org>

layer for 30 keV protons was calculated to be 7.5 keV. The standard deviation of this energy loss (energy straggling) is $\sigma = 0.4$ keV, and the possible variations of proton impact energy and angle change the mean energy loss only by an amount that is much smaller than the energy straggling. The size of the energy loss was also measured on a proton source dedicated for detector tests. It was found that for protons with an impact energy of 30.4 keV the mean energy loss was only 5.8 ± 0.9 keV. A possible explanation would be that the dead layer of our detector is thinner than specified by the company. Using the specified dead layer thickness, we found that 0.3% of the protons are backscattered before they deposit enough energy in the detector to produce a signal. Of interest is the change of the probability of a proton not to be detected with the proton energy, and this is about 400 ppm/keV. For the present data, we can still neglect a correction for the proton detector efficiency. For our recent beam time taken at the ILL in Grenoble, we performed first simulations, because we were using a new proton detector, i.e. use of a silicon drift detector allowed us to significantly reduce the post-acceleration voltage, by a factor of about 2 compared to the previously used silicon PIN diode. Although this simulations show that the effect is rather small, it will be investigated experimentally at the proton source.

Inhomogeneity of the work function of the electrodes {Subtask T-J11-1.2. Systematic effects}

An unexpected systematic error, caused by the inevitable inhomogeneity of the work function of the electrodes (cf. [9,10]), needs further theoretical and experimental studies. A variation of the work function within an electrode, or between different electrodes would render the voltage difference between decay volume and analyzing plane uncertain despite the multimeter measurement. Indeed, a spatial variation of up to 100mV over a distance of several cm was found on a cylindrical sample electrode. If the analyzing plane voltage were measured incorrectly by this amount, the extracted value for α would be wrong by about 1% [13]. In the future, surface coatings and/or treatments for the inner surfaces of our electrode system have to be found which don't show this spatial variation. We suspect that the impurity of our gold surface causes the problem. Sputtered gold surfaces, or different surface materials are reported to give better results. To investigate this effect, further measurements with a Kelvin probe are ongoing.

NMR on-line monitoring {Subtask T-J11-1.2. Systematic effects}

The method of measuring the magnetic field strength with NMR technology is based on the quantization of the spin alignment in a magnetic field. For example the proton spin (1/2) can be aligned parallel or anti-parallel to the magnetic field. This results in two energy levels with an energy gap of $E = \gamma \hbar B$, where B denotes the magnetic field and γ the gyromagnetic ratio. Therefore, a proton for example can only emit or absorb photons of the energy:

$$\Delta E = E_j - E_i$$

According to Planck this corresponds to an electromagnetic wave of the frequency:

$$\nu = \frac{E}{h} = \frac{\gamma \hbar |B|}{h} = \frac{\gamma |B|}{2\pi}$$

where h is Planck's constant. This frequency is called Larmor's frequency, and depends only on the magnetic field. Thus knowing the gyromagnetic ratio a measurement of the frequency can be used to measure the magnetic field strength. The measurement is performed with the help of a probe placed inside the magnetic field. The probe consists of a sample of hyper polarized ^3He which is surrounded by a resonant circuit.

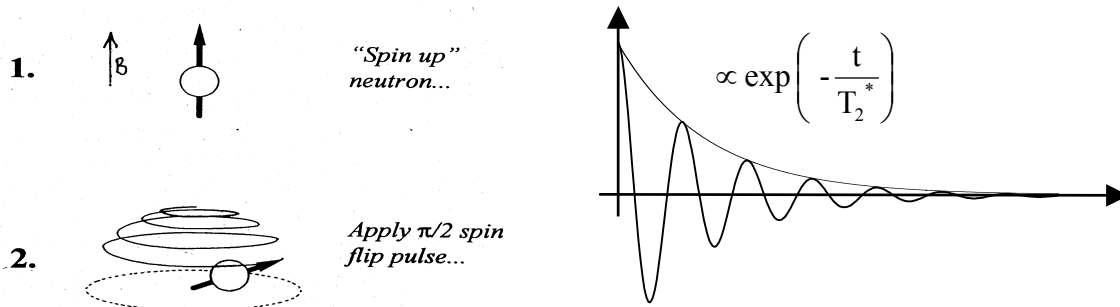


Figure 9: Spin flip with an alternating magnetic field, B_1 .

Figure 10: NMR signal decaying with a time constant T_2 (relaxation time).

A resonant radio frequency (rf) field pulse (B_1) is applied perpendicular to the static field B . Depending on the amplitude (B_1) and the rf pulse duration, the protons spin can be flipped out of the z -axis by an angle α , $\alpha = 2 \pi \gamma \tau B_1$ (Fig. 9). The transverse component of the magnetization, $M^\perp = M_0 \sin \alpha$, is monitored by means of pick up coils which are also perpendicular to the z -axis of the field.

The time constant which describes the return to equilibrium of the transverse magnetization is called the spin-spin relaxation time, T_2 . During this T_2 time, the net perpendicular magnetization decreases in a factor e . The transversal magnetization induces an alternating current in the spin flip coil which decreases as it is shown in figure 10. This signal can be recorded, and from the analysis of its frequency (Larmor frequency), the magnetic field can be extracted with very high accuracy. In the next picture (Fig. 11) it is shown a sketch of the experimental setup for the NMR measurement implemented on the spectrometer.

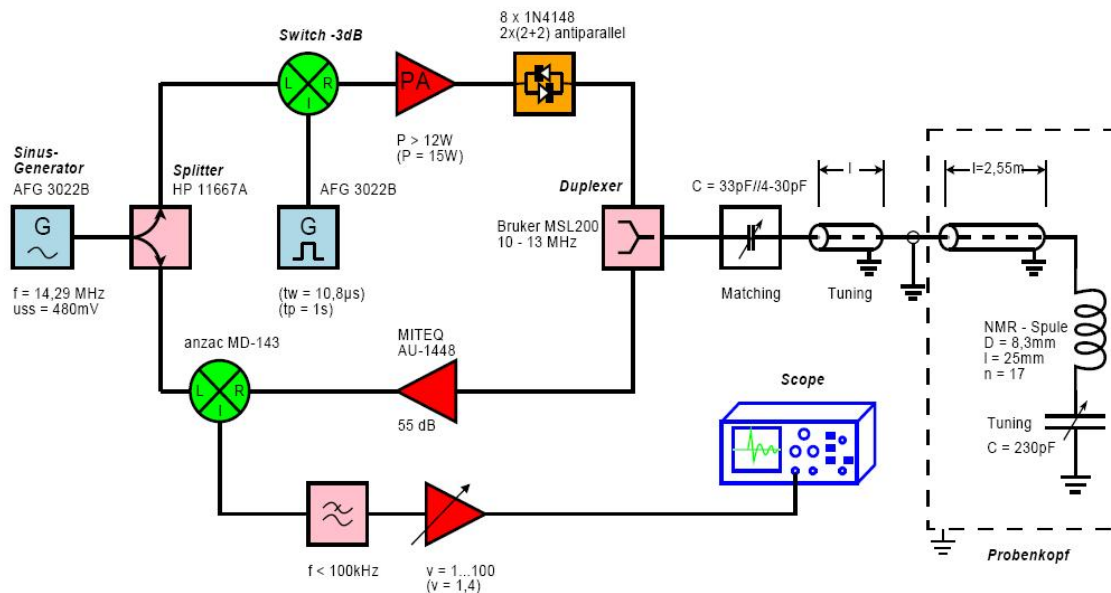


Figure 11: Sketch of the aSPECT NMR system for high accurate measurement of the magnetic field.

For a magnetic field of about 0.44T (value of the field at the decay volume) the radio frequency generator produces a pulse of about 14.3MHz that is amplified and guided by the duplexer through the matching circuit to the resonance circuit (pick-up coil) inside the spectrometer (Fig. 12). The NMR signal received by the pick-up coils travels backwards to

the duplexer and is amplified before to be mixed with a reference signal, in our case via a Lock-in amplifier.



Figure 12: Resonance circuit and glass probe at the analysing plane region. The resonance circuit is an LC circuit that matches to the impedance of the sending-receiving electronics. To fulfil the extreme requirements of UH vacuum and low temperatures the LC components have been designed in vacuum-compatible materials with very similar dilatation coefficients.

The electronics and the working principle have been tested on a NMR magnet with a relative homogeneity similar to *a*SPECT, that is about 10^{-4} (Fig. 13). The results have proved to provide the accuracy required for a precision measurement of *a*. The only limitation found at this point comes from the intrinsic inhomogeneity of the magnetic field generated by the NMR magnet. The atoms sitting along the cell feel a different magnetic field (at 1.3 bar of pressure and room temperature the atoms can be considered stationary during the duration of a single measurement, typically some milliseconds) and therefore precess at a slightly different Larmor frequency. The result is a signal composed as a superposition of all these frequencies with a bandwidth determined by the inhomogeneity of the field. The recovered signal will reflect this spread on the analysis of its frequency, widening therefore the uncertainty on the extracted magnetic field. The typical recovered signal is shown on (Fig. 14)

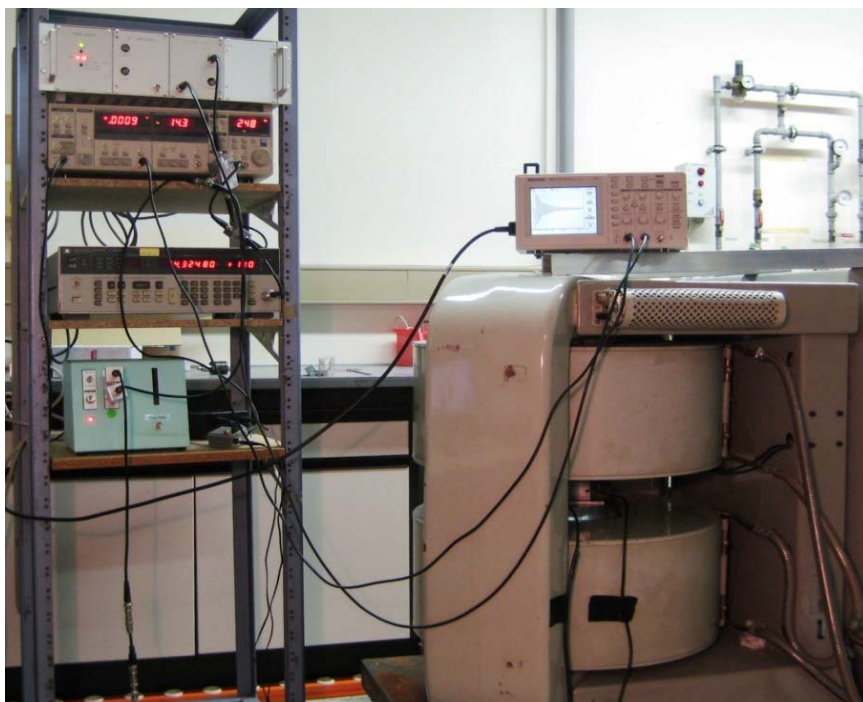


Figure 13: NMR test setup. Left: Radio frequency electronic setup, Right: NMR magnet with pick-up coils and a sample glass cell containing hyperpolarized ^3He .

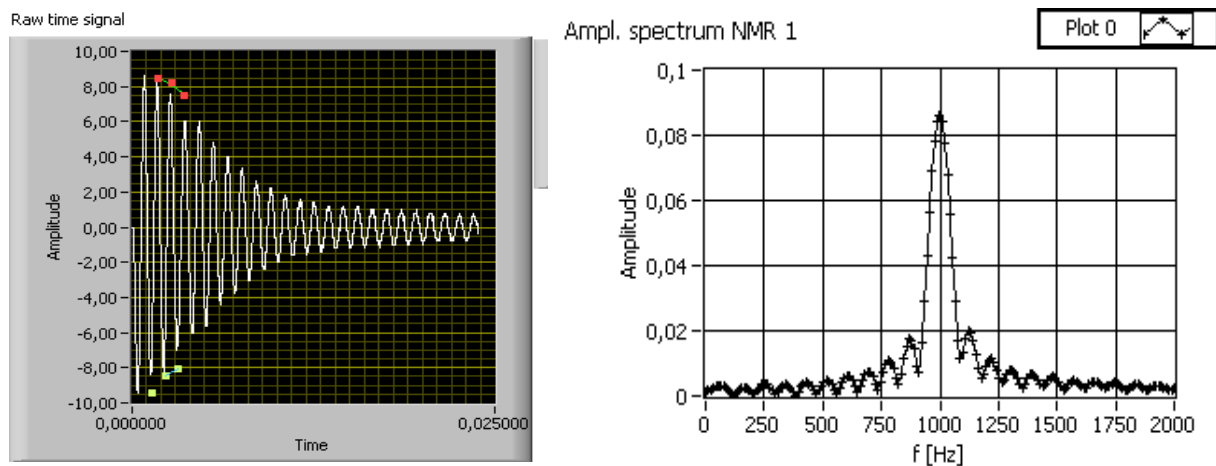


Figure 14: Left: NMR signal recovered for a magnetic field of 0,44185 (10)T and a spin-flip radio frequency pulse of 14,331800 (2) MHz, Right: FFT of the signal. The width of the FFT limits the accuracy on the measurement of the magnetic field.

Data analysis {Subtask T-J11-1.3. Data analysis}

The data analysis of the test beam time performed at the FRM-II reactor in Munich is finished. The PhD thesis of Raquel Muñoz Horta is in progress [1], and a paper about that beam time is already published [10].

In a nutshell, the extracted values of the antineutrino electron angular correlation coefficient a depend on the proton like background signal in the pulse height spectrum. Literature values can be reproduced in case of negligible small background contributions in runs where low HV leakage currents (field emission) were measured. The background can be subtracted in a definite way by measurements with cold neutron beam on and off at the same voltage and magnetic field settings.

Data analysis of the beam time taken at the ILL in Grenoble during April / May 2008 is currently on the way.

Recent publications

- [1] *R. Muñoz Horta*, **First measurements of the aSPECT spectrometer**, doctoral thesis, Johannes-Gutenberg-Universität Mainz, in progress
- [2] *F. Glück*, **Axisymmetric electric field calculation by zonal harmonic expansion**, to be published
- [3] *F. Glück*, **Magnetic field calculation of coils by zonal harmonic expansion**, to be published
- [4] *F. Glück*, **Axisymmetric electric field calculation by BEM and elliptic integrals**, to be published
- [5] *F. Glück*, **Magnetic field calculation of coils by elliptic integrals**, to be published
- [6] *F. Glück*, **3-dimensional electric field calculation by the boundary element method**, to be published
- [7] *F. Glück*, **The Penning discharge**, to be published
- [8] *G. Konrad et al.*, **Magnetic shielding for the aSPECT spectrometer and effect of magnetic materials**, to be published
- [9] *M. Simson et al.*, **Measuring the proton spectrum in neutron decay – latest results with aSPECT**, submitted to NIM
- [10] *S. Baeßler et al.*, **First Measurements with the Neutron Decay Spectrometer aSPECT**, Eur. Phys. J. A **38**, 17-26 (2008)
- [11] *G. Konrad et al.*, **Design of an Anti-Magnetic Screen for the Neutron Decay Spectrometer aSPECT**, Proceedings of the European Comsol Conference, Grenoble, France (2007)
- [12] *F. Ayala Guardia*, **First tests of the neutron decay spectrometer aSPECT**, diploma thesis, Johannes Gutenberg-Universität Mainz (2005)
- [13] *F. Glück et al.*, **The neutron decay retardation spectrometer aSPECT: Electromagnetic design and systematic effects**, Europhys. Journal A **23** (1) (2005) 135-146